IEEE Access
Multidisciplinary | Rapid Review | Open Access Journal

Received July 10, 2019, accepted August 1, 2019, date of publication August 7, 2019, date of current version August 20, 2019.

Digital Object Identifier 10.1109/ACCESS.2019.2933627

Force Ripple Estimation and Compensation of PMLSM With Incremental Extended State Modeling-Based Kalman Filter: A Practical Tuning Method

RUI YANG, LI-YI LI, (Senior Member, IEEE), MING-YI WANG, CHENG-MING ZHANG, AND YI-MING ZENG-GU

Department of Electrical Engineering, Harbin Institute of Technology, Harbin 150001, China

Corresponding author: Li-Yi Li (liliyi.hit@gmail.com)

This work was supported in part by the State Key Program of National Natural Science of China under Grant 51537002, in part by the State Major Program of National Natural Science of China under Grant 51690182, and in part by the National Natural Science of China Youth Fund under Grant 51707046.

ABSTRACT This paper focuses on the force ripple estimation and compensation with the Kalman filter for the permanent magnet linear synchronous machine (PMLSM). The force ripple dynamics is firstly modeled as a higher-order integrator subsystem with fully considering its inherent nonlinear and time-varying characteristic. The motion system dynamics is then extended with modeling the force ripple as an extra state. The main idea for the accurate force ripple estimation is to construct an incremental extended state modeling-based Kalman filter (IESM-KF) for reducing the calculation cost as the higher-order dynamics of the force ripple is considered. And also, a simple and practical parameter tuning method for the IESM-KF is proposed with injecting a square-wave current disturbance to the position controller's output under the cascade position-current closed loop. The inevitable time delay of the mechanical system is estimated with the sine-sweep-based model identification and is further considered in the IESM-KF design. Detailed experimental results are given to validate the effectiveness of the force ripple compensation with the IESM-KF and the corresponding parameter tuning method.

INDEX TERMS Extended state, force ripple, Kalman filter, linear motor, model identification, parameter tuning.

I. INTRODUCTION

Contributed to its prominent direct-drive advantage, the permanent magnet linear synchronous machine (PMLSM) has been devoted to more and more attention especially in the positioning system with requirements of high-speed and high-accuracy [1], [2]. However, compared to its rotary counterpart plus lead screw, the force disturbance including the inherent detent force of the iron-core PMLSM and the external force such as the cable force will be directly exerted on the platform without any buffer [3]. Then the position tracking accuracy will be largely reduced and even vibration and noises can be aroused [1]–[3]. Therefore, significant research efforts have been focused on the analysis, modeling, identification, estimation and compensation of the force ripple [1]–[22], [28], [30], [33]–[35]. The analysis and design method for reducing the detent force of the PMLSM are given from the perspective of optimizing the motor structure, such as in [3]–[7]. With the above methods, the detent force can only be reduced to some extent and it is still large enough for realizing high-accuracy position tracking. Moreover, the complicated motor structure limits its practical application and increases its manufacturing cost. Thus, more and more research efforts have also been devoted to the controller improvement in the control community [1]–[4], [8]–[22], [28], [30], [33]–[35].

As the periodical and repetitive motion characteristic of the linear motion system are fully considered, the iterative

The associate editor coordinating the review of this manuscript and approving it for publication was Min Wang.

learning control [1], [13], [14], the repetitive control [15] and the periodic adaptive learning control [2], [16], [17] are added to the basic feedback control system. The position tracking error has been largely reduced with the growing of iterations. However, the basics of the above learning feedforward control are that the position trajectory and the system states should all be repetitive among each iteration period [1], [2], [13]–[17]. This has limited its general applications especially for the requirements of varying-trajectory [14]. Therefore, there has been large works focusing on the two-degrees-of-freedom (2DOF) control system design with improved feedback and feedforward controller design [18]. An adaptive force ripple compensation method based on the friction and detent force model was proposed in [19], largely-reduced position tracking error has been obtained. However, only the main component of the force ripple was considered in the adaptive control term. In [20] and [21], the adaptive robust control with an adaptive feedforward control for reducing the effect of the main components of the cogging force and a robust term for considering the uncertainty was proposed to improve the force ripple compensation. The same idea has been utilized in [22] where the robust term has been replaced with a sliding mode control. Compared with [19], the methods in [20]–[22] have given more considerations on the higher-order harmonics of the position-dependent cogging force, and thus higher-accuracy position tracking can be expected. The above methods are more or less model-dependent, i.e., the friction and the detent force model are required and then the corresponding model parameters are adapted online. However, explicit representations of the force disturbance are not easy especially as the mechanical installation accuracy and the nominal operation conditions cannot be guaranteed. Therefore, the observer-based 2DOF control has aroused large attention as reviewed in [23]–[25]. Due to its simple-structure and implementation simplicity, the disturbance observer (DOB)-based robust control has been largely utilized in the motion control system design, such as in [26]–[28]. However, its stability and robustness are affected with the parameter variation as analyzed in [29]. And also, some general observer theories have been given considerations for the force ripple compensation as in [3] and [30] where the force ripple was observed from the current input of the motor driver and the position measurement.

Thanks to its optimal estimation characteristic for the linear system [31], [38], the Kalman filter (KF)-based state observer has been expanded for the force ripple estimation as in [32] and [33] where the force ripple was considered as an extra system state. With further considering that the force ripple is position-dependent and can be decomposed up to finite order harmonics, a higher-order system model was constructed with considering the amplitudes of the main harmonics as extended states and then the KF is utilized in [34] to get the optimal estimates. However, the computation burden and the difficulty of parameter tuning increase largely as the order grows. That is to say, the force ripple estimation accuracy and the parameter tuning complexity should be balanced. In [35], the permanent magnet flux linkage was estimated online with the extended Kalman filter (EKF) and then the sampled q-axis current was corrected for reducing the torque ripple. However, the basic assumption is that the permanent magnet flux linkage was slowly-varying, and this has limited its applications due to that the flux is more or less position dependent and time-varying. The detailed parameter tuning procedure was also not given in [32]–[35]. Motivated by the method in [32] and [33] and for further considering the calculation cost reduction, an incremental extended state modeling (IESM) method is proposed in this paper, where the following IESM-KF design for the force ripple estimation and compensation with reduced order can be obtained and then the computation burden can be expected to be largely reduced. Based on the KF parameter tuning method proposed in [36], a simple and practical parameter tuning scheme is also given in detail for the first time with the knowledge of the authors especially for the force ripple estimation. Thus, the blind trial-and-error parameter tuning process can be largely released with our proposed scheme.

The remaining parts of this paper are organized as follows. The plant dynamics with considering the time delay of the mechanical system and the problem statement are given in Section II. The IESM-KF design and the corresponding parameter tuning procedure is analyzed in Section III. Experimental setup and results are given in Section IV. And conclusions are listed in Section V.

II. PLANT DYNAMICS AND PROBLEM STATEMENT

A. PLANT DYNAMICS

As neglecting the rapid electrical dynamics and the high-frequency flexible vibration modes [20], [21], the continuous-time mechanical dynamics of the PMLSM motion system in terms of nominal parameters can be represented as [2]

$$\begin{aligned} M_o \frac{d^2x(t)}{dt^2} &= -B_o \frac{dx(t)}{dt} + F_e(t) - F_d(x, \dot{x}, t), \\ F_e(t) &= K_{fo} i_q(t), \end{aligned} \tag{1}$$

where $x(t)$ is the mover position, M is the total mass of the moving part, B is the viscous friction coefficient, the subscript "o" denotes the nominal value. $F_e(t)$ is the electromagnetic force as the vector control with $i_d^* = 0$ is utilized and $K_{fo} = (3\pi/2\tau)\,\psi_{fo}$ is the thrust coefficient in which τ is the pole-pitch, ψ_f is the permanent magnet flux linkage. $F_d(x, \dot{x}, t)$ is the lumped force disturbance which can be described as

$$\begin{aligned} F_d(x, \dot{x}, t) = &-\Delta K_f i_q(t) + \Delta M \frac{d^2x(t)}{dt^2} - \Delta B \frac{dx}{dt} \\ &+ F_{fric}(x, \dot{x}) + F_r(x) \\ &+ F_{ext}(x, \dot{x}, t) + \varepsilon_F, \end{aligned} \tag{2}$$

where $F_{fric}(x, \dot{x})$ is the Coulomb friction force, $F_r(x)$ is the inherent force ripple of the iron-core PMLSM, which is mainly comprised of the detent force, the effect of the current/flux distortions and the current offsets; $-\Delta K_f i_q(t) + \Delta M \frac{d^2x(t)}{dt^2} - \Delta B \frac{dx}{dt}$ denotes the coupling effect of the parameter variation with the system states, in which

$\Delta K_f = K_f - K_{fo}$, $\Delta M = M - M_o$, $\Delta B = B - B_o$ are the parameter mismatch against the nominal value; $F_{ext}(x, \dot{x}, t)$ is the external force disturbance such as the cable force [1] and the equivalent load force (which can be caused by the inclination of the base frame) and ε_F is the un-modeled force. For simplicity, the suffix is omitted hereafter and (1) is rearranged as

$$M_o\ddot{x} = -B_o\dot{x} + K_{fo}(u + u_d), \tag{3}$$

where $u = i_q$ is the actual q-axis current and $u_d = -F_d/K_{fo}$ is the equivalent q-axis current disturbance due to the lumped force F_d. Due to the existence of the calculation delay of the control algorithm, the driver/actuator system dynamics and the position measurement delay, the mechanical system delay is inevitable [1]. As the time delay is considered, the transfer function of the PMLSM motion system with model (3) can be represented again in the Laplace domain as

$$P(s) = \frac{Y(s)}{U(s)} = \frac{K_{fo}}{M_o s^2 + B_o s} e^{-t_d s}, \tag{4}$$

where s denotes the Laplace operator, y is the measured output of the position x, and t_d is the aforementioned time delay. The simplified diagram is shown in Fig. 1.

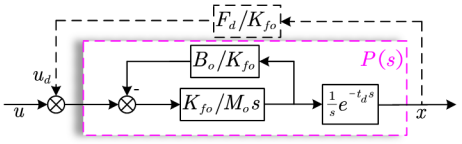

FIGURE 1. Simplified block diagram of the PMLSM motion system.

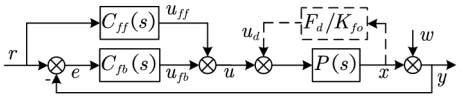

FIGURE 2. General block diagram of the PMLSM motion control system with feedback control based on the position tracking error and feedforward control based on the reference trajectory.

B. PROBLEM STATEMENT

As shown in (1) or (2), if the parameters M_o, B_o, K_{fo} are given, the motion control system with the general feedback and feedforward control terms i.e., $C_{fb}(s)$ and $C_{ff}(s)$ as depicted in Fig. 2 can be designed with the given performance requirements. Also, if the accurate expression of the disturbance u_d is known, an explicit feedforward can be made and the trajectory tracking accuracy can be improved further. It can be noted from (2) that the force disturbance $F_d(x, \dot{x}, t)$ is nonlinear and time-varying, i.e., $\dot{F}_d(x, \dot{x}, t) \neq 0$; this is also one of the starting points of this paper. Thus, the main problems for the linear motion system design lie on the accurate model parameter identification and the real-time/high-accuracy compensation of the time-varying force disturbance.

Motivated by the Kalman filter-based state observer proposed in [32] and [33], an incremental extended-state modeling-based KF is proposed and a simple but practical parameter tuning method is also given in detail in the first time to the knowledge of the authors. The main focuses of this paper are: (1) how to reduce the order and then the computation cost of the Kalman filter as the higher-order dynamics of the force ripple is considered for the following accurate estimation and compensation, (2) and how to tune the KF parameters easily just like the general regulation of the PI-based controller.

III. IESM-KF DESIGN AND PARAMETER TUNING FOR THE FORCE RIPPLE COMPENSATION

A. EXTENDED STATE MODELLING

According to (2), with neglecting the Coulomb friction force $F_{fric}(x, \dot{x})$ and the un-modeled force ε_F of the air-bearing PMLSM, the lumped force disturbance can be expanded locally with the Taylor polynomial with respect to time as following [39]:

$$F_d = K_{fo}\left(\sum_{j=0}^{n-1} a_j t^j + \eta(t)\right), \tag{5}$$

where n is the order, a_j $(j = 0,1,\ldots, n-1)$ are the polynomial coefficients, $\eta(t)$ represents the residual high-frequency parts with smaller and bounded consecutive-time-derivatives, such as the smaller neglected friction force on speed reversal motion and the high-frequency components of the force ripple, i.e., $|\eta^{(k)}(t)| \approx 0, k = 0,\ldots, n-1$ and $|f_{dq}^{(k)}(t)| = |\eta^{(k)}(t)| \approx 0$ as $k \geq n$ [39]. This means that the low-frequency parts of the nonlinear disturbance are simply modeled as a polynomial with finite order and the high-frequency components are neglected. Thus, the disturbance dynamics is approximated as the following nth-order integrator subsystems:

$$\left.\begin{aligned} u_d^{(1)} &= \underbrace{\sum_{j=1}^{n-1} j a_j t^{j-1}}_{=h_d^1} \\ u_d^{(2)} &= \underbrace{\sum_{j=2}^{n-1} j(j-1) a_j t^{j-2}}_{=h_d^2} \\ &\vdots \\ u_d^{(n)} &= \underbrace{0}_{=h_d^n} \end{aligned}\right\}, \tag{6}$$

then (3) and (6) can be rearranged as the following $(n+2)$th-order extended state model:

$$\left.\begin{aligned} \dot{x} &= v \\ \dot{v} &= -B_o/M_o v + K_{fo}/M_o (u + u_d) \\ u_d^{(1)} &= h_d^1 \\ &\vdots \\ u_d^{(n)} &= h_d^n \end{aligned}\right\}, \tag{7}$$

where $h_d^{(j)}, j = 1,\ldots, n$ denote the j-th time-derivatives of u_d. With the state-space representation, (7) can be simplified to the following form:

$$\left.\begin{aligned} \dot{\boldsymbol{x}} &= \boldsymbol{A}\boldsymbol{x} + \boldsymbol{B}u + \boldsymbol{w} \\ y &= \boldsymbol{C}\boldsymbol{x} + \zeta \end{aligned}\right\}, \tag{8}$$

where $\boldsymbol{x} = \left[x\ v\ u_d \ldots u_d^{(n-1)}\right]^T_{1\times(n+2)}$ is the state vector, $\boldsymbol{w} = [w_1\ w_2 \ldots w_{n+2}]^T_{1\times(n+2)}$ is a random process noise vector with the variance $\sigma_1^2, \ldots, \sigma_{n+2}^2$, ζ is the measurement noise which is generally white-Gaussian distributed with the variance σ_R^2, y is the position measurement output, and the system matrices are

$$\boldsymbol{A} = \begin{bmatrix} 0 & 1 & 0 & 0 & \cdots & 0 & 0 \\ 0 & -B_o/M_o & K_{fo}/M_o & 0 & \cdots & 0 & 0 \\ 0 & 0 & 0 & 1 & \cdots & 0 & 0 \\ \vdots & \vdots & \vdots & \vdots & \ddots & 0 & 0 \\ 0 & 0 & 0 & 0 & 0 & 1 & 0 \\ 0 & 0 & 0 & 0 & 0 & 0 & 1 \\ 0 & 0 & 0 & 0 & 0 & 0 & 0 \end{bmatrix}_{(n+2)\times(n+2)},$$

$$\boldsymbol{B} = \begin{bmatrix} 0 & K_{fo}/M_o & 0 \ldots 0 \end{bmatrix}^T_{(n+2)\times 1},$$

$$\boldsymbol{C} = [1 \quad 0 \ldots 0]_{1\times(n+2)}.$$

As the zero-order-hold (ZOH) method is used, (8) can be discretized as

$$\left.\begin{aligned} \boldsymbol{x}(k+1) &= \boldsymbol{A}_d\boldsymbol{x}(k) + \boldsymbol{B}_d u(k) + \boldsymbol{G}_d\boldsymbol{\omega}(k) \\ y(k) &= \boldsymbol{C}_d\boldsymbol{x}(k) + \zeta(k) \end{aligned}\right\}, \tag{9}$$

where the matrices are [38]

$$\begin{aligned} \boldsymbol{A}_d &= e^{\boldsymbol{A}T_s} = \sum_{i=0}^{n} \frac{1}{i!}(\boldsymbol{A}T_s)^i, \\ \boldsymbol{B}_d &= \int_0^{T_s} e^{\boldsymbol{A}\tau}\boldsymbol{B}d\tau, \\ \boldsymbol{G}_d &= \int_0^{T_s} e^{\boldsymbol{A}\tau}d\tau, \\ \boldsymbol{C}_d &= \boldsymbol{C}, \end{aligned} \tag{10}$$

and the process covariance matrix is [38]

$$\begin{aligned} \boldsymbol{Q} &= \int_0^{T_s} e^{\boldsymbol{A}\tau} E\left[\boldsymbol{w}\boldsymbol{w}^T\right] e^{\boldsymbol{A}^T\tau} d\tau \\ &= \int_0^{T_s} e^{\boldsymbol{A}\tau}\,\mathrm{diag}\left(\sigma_1^2, \ldots, \sigma_{n+2}^2\right) e^{\boldsymbol{A}^T\tau} d\tau, \end{aligned} \tag{11}$$

It can be noted that (9) is a linear uncertain dynamic system with constant matrices $\boldsymbol{A}_d, \boldsymbol{B}_d, \boldsymbol{G}_d$ and $\boldsymbol{C}_d$. Thus, the optimal state estimation of $\boldsymbol{x}_e$ can be realized here with the classical KF [37]. However, as the order of the disturbance dynamics model (5) increases, the calculation burden of the KF also grows largely. Therefore, there exists a balance between the accuracy of the disturbance modeling and the computation cost. To release this balance, an incremental extended state modeling method is proposed in the following.

B. IESM-KF DESIGN

According to (9), the system model in the $(k-1)$th instant is

$$\left.\begin{aligned} \boldsymbol{x}(k) &= \boldsymbol{A}_d\boldsymbol{x}(k-1) + \boldsymbol{B}_d u(k-1) + \boldsymbol{G}_d\boldsymbol{\omega}(k-1) \\ y(k-1) &= \boldsymbol{C}_d\boldsymbol{x}(k-1) + \zeta(k-1) \end{aligned}\right\}, \tag{12}$$

and then subtracting (9) from (12), the discrete IESM can be obtained as

$$\left.\begin{aligned} \Delta\boldsymbol{x}(k+1) &= \boldsymbol{A}_d\Delta\boldsymbol{x}(k) + \boldsymbol{B}_d\Delta u(k) + \boldsymbol{G}_d\Delta\boldsymbol{\omega}(k) \\ \Delta y(k) &= \boldsymbol{C}_d\Delta\boldsymbol{x}(k) + \Delta\zeta(k) \end{aligned}\right\}, \tag{13}$$

where $\Delta vec(k) = vec(k) - vec(k-1)$ denotes the increment of the vector vec. Considering the disturbance dynamics (6) again, it can be found that the n-th order dynamics of $u_d^{(n)} = 0$ is equivalent to $u_d^{(n-1)}(k) - u_d^{(n-1)}(k-1) = 0$, i.e., $\Delta u_d^{(n-1)}(k) = 0$. Thus, the IESM can be reduced to the following $(n+1)$-order one as:

$$\left.\begin{aligned} \Delta\boldsymbol{x}'(k+1) &= \boldsymbol{A}'_d\Delta\boldsymbol{x}'(k) + \boldsymbol{B}'_d\Delta u(k) \\ &\quad + \boldsymbol{G}'_d\Delta\boldsymbol{\omega}'(k) \\ \Delta y(k) &= \boldsymbol{C}'_d\Delta\boldsymbol{x}'(k) + \Delta\zeta(k) \end{aligned}\right\}, \tag{14}$$

where $\Delta\boldsymbol{x}' = \left[\Delta x\ \Delta v\ \Delta u_d \ldots \Delta u_d^{(n-2)}\right]^T_{1\times(n+1)}$, $\Delta\boldsymbol{w}' = [\Delta w_1\ \Delta w_2 \ldots \Delta w_{n+1}]^T_{1\times(n+1)}$, the matrices $\boldsymbol{A}'_d, \boldsymbol{B}'_d, \boldsymbol{G}'_d$ are the submatrices of $\boldsymbol{A}_d, \boldsymbol{B}_d, \boldsymbol{G}_d$ with eliminating its final row and final column, and $\boldsymbol{C}'_d$ is the submatrix of $\boldsymbol{C}_d$ with eliminating its final column. That is to say, the IESM (which is $(n+1)$-order) is the exact reduced-order version of the ESM (which is $(n+2)$-order).

As $\boldsymbol{w}, \zeta$ are random processes, the deviation $\Delta\boldsymbol{w}, \Delta\boldsymbol{w}', \Delta\zeta$ are also random processes [37]. The covariance matrices of $\Delta\boldsymbol{w}'$, $\Delta\zeta$ are [38]

$$\begin{aligned} \boldsymbol{Q}' &= \int_0^{T_s} e^{\boldsymbol{A}'\tau} E\left[\boldsymbol{w}\boldsymbol{w}^T\right] e^{\boldsymbol{A}'^T\tau} d\tau \\ &= \int_0^{T_s} e^{\boldsymbol{A}'\tau}\,\mathrm{diag}\left(\sigma_1^2, \ldots, \sigma_{n+1}^2\right) e^{\boldsymbol{A}'^T\tau} d\tau \geq 0, \\ R' &= E\left((\Delta\zeta)^2\right) > 0, \end{aligned} \tag{15}$$

Therefore, the basic KF theory can also be utilized here to estimate the incremental states optimally. The recursive implementation procedure of the IESM-KF algorithm is given as follows [31], [37].

The time update step: a priori prediction

(1) State prediction

$$\Delta\boldsymbol{x}'_p(k+1) = \boldsymbol{A}'_d\Delta\boldsymbol{x}'_e(k) + \boldsymbol{B}'_d\Delta u(k), \tag{16}$$

where $\Delta\boldsymbol{x}'_p(k+1)$ is the state prediction at time $k+1$ and $\Delta\boldsymbol{x}'_e(k)$ is the previously deduced state estimation at time k.

(2) Prediction error covariance matrix calculation

$$\boldsymbol{P}_p(k) = \boldsymbol{A}'_d\boldsymbol{P}_e(k-1)\boldsymbol{A}'^T_d + \boldsymbol{Q}', \tag{17}$$

where $\boldsymbol{P}_p(k)$ is the prediction error covariance matrix at time k and $\boldsymbol{P}_e(k-1)$ is the estimation error covariance matrix at time $k-1$, $\boldsymbol{Q}'$ is the covariance matrix of the process noise.

(3) Kalman gain calculation

$$\boldsymbol{K}(k)=\boldsymbol{P}_p(k)\boldsymbol{C}_d^{'T}\left(\boldsymbol{C}_d^{'T}\boldsymbol{P}_p(k)\boldsymbol{C}_d^{'T}+R'\right)^{-1}, \quad (18)$$

where R' is the covariance matrix of the measurement noise.

The measurement update step: a posteriori correction

(4) Estimation update with measurement

$$\Delta\boldsymbol{x}_e'(k+1)=\Delta\boldsymbol{x}_p'(k+1)+\boldsymbol{K}(k)\left(\Delta y(k)-\boldsymbol{C}_d'\Delta\boldsymbol{x}_p'(k)\right), \quad (19)$$

(5) Estimation error covariance matrix update

$$\boldsymbol{P}_e(k)=\left(\boldsymbol{I}-\boldsymbol{K}(k)\boldsymbol{C}_d'\right)\boldsymbol{P}_p(k), \quad (20)$$

(6) Return to (1).

As the comparison analysis of calculation complexity for the variants of the EKF in [40] (Table I in [40]), the calculation burden is approximately proportional to the cube of the state dimensionality and so it will be largely reduced with the above proposed IESM method especially under higher-order disturbance modeling.

For the following parameter tuning, the observability of the extended PMLSM motion system $\left\{\boldsymbol{A}_d', \boldsymbol{C}_d'\right\}$ is verified firstly through checking the rank of the following observability matrix:

$$\boldsymbol{O}=\begin{bmatrix}\boldsymbol{C}_d'\\ \boldsymbol{C}_d'\boldsymbol{A}_d'\\ \vdots\\ \boldsymbol{C}_d'\left[\boldsymbol{A}_d'\right]^n\end{bmatrix}. \quad (21)$$

The model $\left\{\boldsymbol{A}_d', \boldsymbol{C}_d'\right\}$ is observable if and only if the observability matrix $\boldsymbol{O}$ is full-rank, i.e., $rank(\boldsymbol{O})=n+1$ [37]. The above observability condition can be verified offline due to that the matrices $\boldsymbol{A}_d'$ and $\boldsymbol{C}_d'$ are constant as n is selected. The convergence and stability of the IESM-KF can be easily verified with the method in [42] as the time-invariant parameter matrices and linear system are considered.

According to the definition of the incremental states, as they are estimated with the above IESM-KF algorithm, the actual state estimations of (14) can be calculated with

$$\boldsymbol{x}_e'(k)=\boldsymbol{x}_e'(0)+\sum_{i=1}^{k}\Delta\boldsymbol{x}_e'(i), \quad (22)$$

where $\boldsymbol{x}_e'=\left[x\ v\ u_d\ldots u_d^{(n-1)}\right]_{1\times(n+1)}^T$ is the actual state estimations, and $\boldsymbol{x}_e'(0)$ is the initial state estimations of which the selection will be discussed in the following parameter tuning procedure. Considering the time delay effect of the mechanical system (4), the force ripple compensation based on (16)-(20), (22)-(23) is shown in Fig. 3, where m denotes the time delay in terms of the number of the sampling period T_s, it's defined in this paper as

$$m=floor(t_d/T_s), \quad (23)$$

where the function $floor(x)$ gives the greatest integer less than or equal to x.

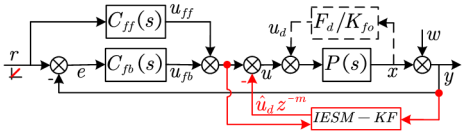

FIGURE 3. Block diagram for the force ripple compensation based on the IESM-KF.

C. IESM-KF PARAMETER TUNING

The main parameters of the IESM-KF to be tuned are $\Delta\boldsymbol{x}_e'(0)$, $\boldsymbol{P}_e(0)$, $\boldsymbol{Q}'$, R' and $\boldsymbol{x}_e'(0)$. Due to that the position sampling and control period is little enough, i.e., $T_s=200\mu s$ as will be designed in this paper, so that $\Delta\boldsymbol{x}_e'(0)=\boldsymbol{0}_{1\times(n+1)}$ can be selected. Considering that the initial estimation error covariance will just affect the transient response of the state estimation, $\boldsymbol{P}_e(0)=\boldsymbol{0}_{(n+1)\times(n+1)}$ can be simply designed without deteriorating the steady-state performance [36].

At the standstill, $x(0)$ can be initialized with the measured position directly as the position encoder's resolution/accuracy is high or assigned with the filtered position with a LPF as a low-resolution position sensor is configured; the velocity, the disturbance and its consecutive time-derivatives can be simply initialized as zeros, i.e., $\boldsymbol{x}_e'(0)=[x(0)\ \ 0\ldots0]_{1\times(n+1)}^T$. Most importantly, the performance of the KF is mainly determined by the parameters $\boldsymbol{Q}'$ and R' [36], of which the tuning is one of the main focuses of this paper.

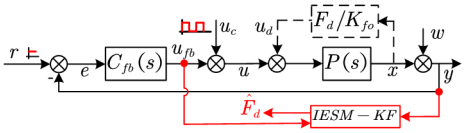

FIGURE 4. Block diagram for the IESM-KF parameter tuning.

Due to that the actual force ripple is not known, there exists no reference for evaluating the effectiveness of the tuned KF parameters. As is shown in Fig. 4, the block diagram for tuning the IESM-KF parameters is proposed in this paper. The position command is set as a constant value, for example the standstill position $x(0)$. The square-wave current command u_c is injected as the input disturbance behind the position feedback controller's output u_{fb}. The inputs of the IESM-KF are selected as u_{fb} and the measured position y. Thus, as robust and high-bandwidth current loop is guaranteed, the electrical dynamics can be neglected, i.e., $i_q^*=i_q$ can be assumed among the position control period where i_q^* is the q-axis current command, the estimated disturbance $\hat{F}_d$ is expected to be

$$\begin{aligned}\hat{F}_d&=K_{fo}(u_c+u_d)\\&=K_{fo}u_c+F_d(x(0)),\end{aligned} \quad (24)$$

Furtherly, considering that there exists no exerted electromagnetic thrust force for maintaining the mover at the standstill position, so $F_d(x(0))$ approaches to zero. Then, as the position deviation from the standstill is little enough, (24) can be

represented as

$$\hat{F}_d \approx K_{fo} u_c. \tag{25}$$

That is to say, if the position command is set as the standstill position, the estimated force disturbance from Fig. 4 is an amplification of the injected current disturbance u_c with a ratio of K_{fo}. Therefore, the waveform of $K_{fo}u_c$ can be seen as a reference for the parameter tuning of the IESM-KF just like the parameter tuning procedure of the traditional PI-based controller. Under this scheme, the blind trail-and-error process for the tuning of the main parameters of $\boldsymbol{Q}'$ and R' can be avoided. The detailed tuning results are given in Section IV.

IV. EXPERIMENTAL EVALUATION

In this section, the basic experimental setup, the plant model identification, the force ripple estimation with the position controller's output, the force ripple compensation with the proposed IESM-KF and the corresponding parameter tuning method are discussed.

A. EXPERIMENTAL SETUP

To verify the effectiveness of the proposed method, as depicted in Fig. 5, an air-bearing test platform for the semiconductor equipment with a surface-mounted iron-core PMLSM was built.

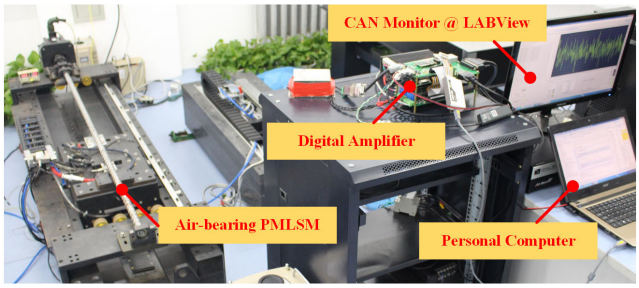

FIGURE 5. The air-bearing PMLSM test platform.

The motor was driven with a full digital power amplifier based on the 32-bit floating-point TI microcontroller (MCU) TMS320F28377D with double cores. The simplified block diagram of the overall system is shown in Fig. 6 and the detailed hardware and software designs are listed below.

1) HARDWARE DESIGN

The amplifier utilizes a three-phase voltage-source-inverter (VSI) with three sets of insulated-gate-bipolar-transistors (IGBTs) under the bus voltage of 310[V], which is rectified from a single-phase AC power supply (220V /50Hz). The switching frequency is selected as 10kHz. The sampling and update frequency of the position and the current loop are 5kHz and 20kHz (in which the double-sampling-double-update scheme for the current loop is utilized), respectively. Two-phase motor currents are measured through two LEM

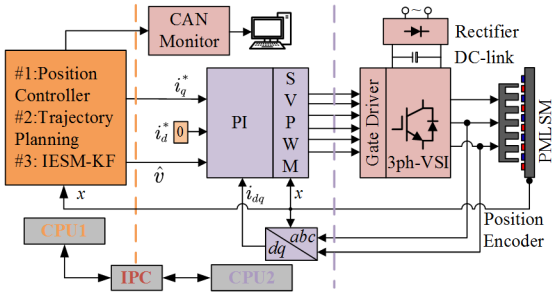

FIGURE 6. Simplified block diagram of the overall control system.

current sensors with the accuracy of ±0.2%. The mover position is measured through a high-resolution (0.1μm) optical linear encoder from Renishaw. Tested results are recorded through the LabVIEW monitor with the CAN2.0 protocol, and then postprocessed using the MATLAB.

2) SOFTWARE DESIGN

The CPU1 of the MCU is configured for the outer position closed loop including the trajectory planning, the position controller implementation, the IESM-KF algorithm and the CAN2.0 protocol. The CPU2 is allocated for the vector control including the current sampling and its postprocessing, the coordinate transformations, the SVPWM, and the PI current controllers, etc. The information request and share between the two CPUs is allowed through the build-in Inter-Processor Communication (IPC) module.

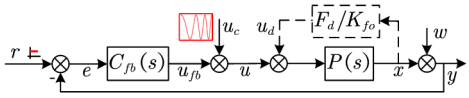

FIGURE 7. Block diagram for the PMLSM model identification.

B. EXPERIMENTAL RESULTS

1) MODEL PARAMETER IDENTIFICATION

As generally used in the control engineering practice, the chirp signal is selected in this paper as the external excitation source for the PMLSM model parameter identification, where the amplitude (5[A]) is maintained constant and the frequency varies exponentially with time from 0.1Hz to 500Hz. The block diagram as shown in Fig. 7 is designed here where the chirp signal is added to the position controller's output and the position reference is set as a fixed position. The actual input of the plant, i.e., $u = u_{fb} + u_c$, and the measured position are recorded for the following estimation of the plant transfer function.

Due to that the position reference is fixed, the feedforward control $C_{ff}(s)$ is of no effect and so it is omitted here. The feedback control $C_{fb}(s)$ is preliminarily designed with a low bandwidth using the nominal model parameters as listed in Table. 1, so as to amplify the effect of the equivalent input disturbance u_c on the position deviation from the setpoint,

TABLE 1. Nominal and identified parameters of the tested PMLSM.

Parameters	Values	Unit
Thrust coefficient/K_{fo}	94.2	N/A
Mover mass/M_o	45	kg
Stator resistance/R_{so}	6.5	Ω
Stator inductance/L_{so}	35	mH
Magnetic flux/ψ_{fo}	0.24	Wb
Pole-pitch (N-S)/τ	12	mm
Identified M/K_f	0.483	kg/(N/A)
Identified Time Delay t_d	844.2	μs

i.e., increase the SNR (Signal to Noise Ratio). The rule of thumb for the position controller design with a PI controller plus a lead compensator and a second-order LPF as expressed in [41] is used here as:

$$C_{fb}(s) = K_p\left(1+\frac{\omega_i}{s}\right)\left(\frac{\alpha s+\omega_c}{s+\alpha\omega_c}\right)\left(\frac{\omega_l^2}{s^2+2\zeta\omega_l s+\omega_l^2}\right), \tag{26}$$

where ω_c is the 0-dB cutoff frequency of the loop gain $L(s) = C(s)P(s)$ (which is generally defined as the controller bandwidth in motion control system [41]), ω_i and ω_l are the corner frequency of the PI controller and the LPF, respectively; α determines the effective frequency range of the lead compensator and then the phase margin; ζ is the damping ratio of the second-order LPF and $K_p = \left(M_o\omega_c^2 + B_o\omega_c\right)/K_{fo}$ is the gain for maintaining the cutoff frequency at ω_c. For the model identification, the above parameters are designed as $\omega_c = 2\pi f_c, f_c = 30Hz, \omega_i = 0.1\omega_c, \omega_l = 10\omega_c, \alpha = 9, \zeta = 0.7$. Then the Tustin method is used to discretize the controller (26) with the sampling period $T_s = 200\mu s$.

The frequency response of the measured input-output data and the identified results are shown in Fig. 8. Considering that the friction force of the tested air-bearing platform is little enough to be neglected, which has also been verified with the identified results, a simplified model with a pure second-order integrator plus a time delay as utilized in [1] is also used here. As shown in the middle subplot of Fig. 8, the time delay contributes to the increased phase delay as the frequency increases and it is estimated with the least square (LS) method using the frequency and phase data below the -180 deg phase line as shown in the bottom subplot of Fig. 8 [1]. The identified value of M/K_f and t_d along with the main motor parameters are listed in Table. 1. The identified M/K_f is larger than the nominal value, i.e., $M_o/K_{fo} = 0.478$kg/(N/A), which can be caused by the increased mover mass due to the added auxiliary mechanical structure. With the identified value, the model-based acceleration feedforward control is simply designed here as

$$C_{ff}(s) = M/K_f s^2. \tag{27}$$

And as the acceleration a is planned, the feedforward control term is simply given as $u_{ff} = M/K_f a$.

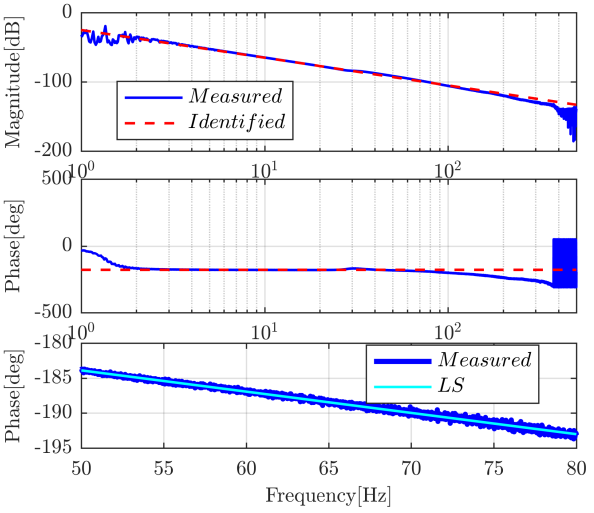

FIGURE 8. Measured and identified frequency response. The time delay is estimated with the phase response under the -180ř line using the least square (LS) method.

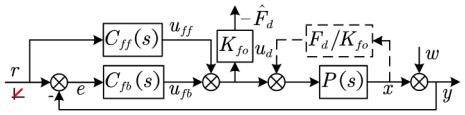

FIGURE 9. Block diagram for the force ripple estimation of the PMLSM.

2) FORCE RIPPLE ESTIMATION

The force ripple of the PMLSM is generally position-dependent and its frequency in the time-domain is proportional to the mover velocity [1]–[7]. With a higher-bandwidth position controller, the force ripple can be rejected to a large extent especially at low velocity. Thus, the characteristic of the force ripple can be represented with the position controller's output indirectly [1], which is depicted in Fig. 9, where the force ripple is estimated as

$$\hat{F}_d = -\left(u_{fb} + u_{ff}\right)K_{fo}. \tag{28}$$

The reference trajectory is designed as a second-order S-curve with the range of $240mm$ $(= 20\tau)$, constant velocity of $20mm/s$ and limited acceleration of $200mm/s^2$. An example of the position trajectory is shown in Fig. 10, where the position, velocity and acceleration are normalized against their corresponding maximum values. The position controller's bandwidth of (26) is increased to $60Hz$ and the other parameters are the same with the one for the above model identification.

The force ripple estimation results are shown in Fig. 11. It can be noted from Fig. 11 (a) that the maximum position tracking error is $\pm 3\mu m$ (about 0.025% of the pole-pitch), so the force ripple can be estimated with the position controller's output to some extent. For reducing the noise effect, the estimated force is filtered with a sixth-order zero phase LPF (ZPLPF) as shown in the bottom subplot of Fig. 11 (a)

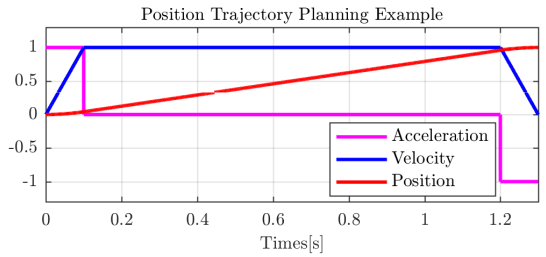

FIGURE 10. An example of the second-order position trajectory.

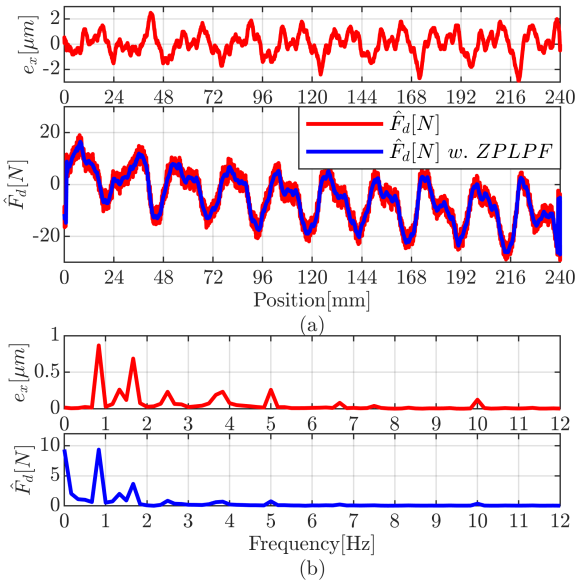

FIGURE 11. Force ripple estimation results. (a) The position tracking error and the estimated force ripple before and after postprocessing with a sixth-order ZPLPF (the cutoff frequency is 50Hz), (b) the FFT results of the position error and the force ripple.

TABLE 2. Main harmonics of the force ripple estimation FFT results.

Frequency[Hz]	Order	Amplitude[N] w. o. IESM-KF	Amplitude[N] w. IESM-KF
0	0	9.374	10.18
0.833	**1**	**9.352**	**9.347**
1.333	1.5	1.995	2.05
1.664	2	3.657	3.666
2.494	3	0.851	0.899
3.333	4	0.142	0.127
3.822	4.5	0.702	0.665
4.997	6	0.760	0.740
6.669	8	0.224	0.225
7.516	9	0.087	0.103
9.992	12	0.363	0.313

and the FFT results of the filtered force is shown in the bottom subplot of Fig. 11 (b) (where the data between the position range of $[80, 200]mm$ is analyzed and it's also conducted in the following analysis). The main frequency components of the force ripple are listed in Table. 2, in which the DC offset, the fundamental frequency of $0.833Hz(= 20/(2\tau))$ and its second-order harmonics are dominant. It can be seen in the bottom subplot of Fig. 11 (a) that the force offest

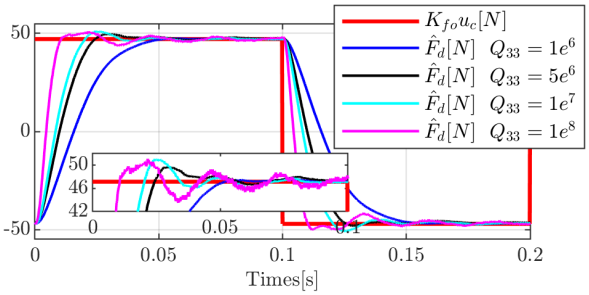

FIGURE 12. The response performance of estimated $\hat{F}_d$ with respect to the injected square-wave disturbance $K_{fo}u_c$ with $Q_{11} = 0.01$, $Q_{22} = 100$, $R' = 1e^{-6}$ and Q_{33} varying within $[1e^6, 1e^8]$.

increases with the position which can be caused by the gravity component due to the inclination of the marble base. Then the offset current is required to overcome this equivalent load force. Thus, the estimated force disturbance will be composed of the detent froce (of which the theoretical position period is just τ [1], [3], [5], [6]) and the extra force ripple caused by the offset current. Therefore, the estimated results can be expected to be not consistent with our previous publication [3]. The main frequency components of the FFT results for the position tracking error are the same as the force ripple, which has reflected the limitations of the feedback control due to that the control effort can just be active after the error occurs and this contributes to the phase delay of the control effect. With our proposed IESM-KF-based force ripple estimation/compensation method, the periodical position errors can be largely reduced as will be given in the following tests.

3) IESM-KF PARAMETER TUNING

As analyzed in Section III. C, $\Delta \boldsymbol{x}_e'(0) = \mathbf{0}_{1\times(n+1)}$, $\boldsymbol{P}_e(0) = \mathbf{0}_{(n+1)\times(n+1)}$ and $\boldsymbol{x}_e'(0) = [x(0)\ \ 0\ldots 0]^T_{1\times(n+1)}$ are designed. Thus, the remaining work is focused on the tuning of $\boldsymbol{Q}'$ and R'. The amplitude and frequency of the square-wave current u_c in Fig. 4 are 0.5[A] and 5[Hz], respectively. As $n = 2$ is selected, i.e., $u_d^{(2)} = 0$ is assumed, the matrix $\boldsymbol{Q}' = \text{diag}(Q_{11}, Q_{22}, Q_{33})$ and the variance R' are to be tuned. The observability of $\{\boldsymbol{A}_d', \boldsymbol{C}_d'\}$ is verified with substituting the identified parameters in MATLAB code. Then, the single-variable-method is utilized here and the variables $K_{fo}u_c$ and $\hat{F}_d$ are recorded and analyzed for optimizing the KF parameters.

Fig. 12 shows the response performance of the estimated $\hat{F}_d$ with respect to the injected square-wave disturbance $K_{fo}u_c$ with maintaining $Q_{11} = 0.01, Q_{22} = 100, R' = 1e^{-6}$ unchanged and Q_{33} varying within $[1e^6, 1e^8]$. It can be seen that as Q_{33} increases, the convergence of $\hat{F}_d$ also accelerates; while the overshoot and oscillation also aggravates as depicted in the magnified subplot of Fig. 12. Figs.13 and 14 show the response performance of the estimated $\hat{F}_d$ with Q_{22} and Q_{11} varying, respectively. As can be seen, the convergence of $\hat{F}_d$ accelerates with the decrease of Q_{11} or Q_{22},

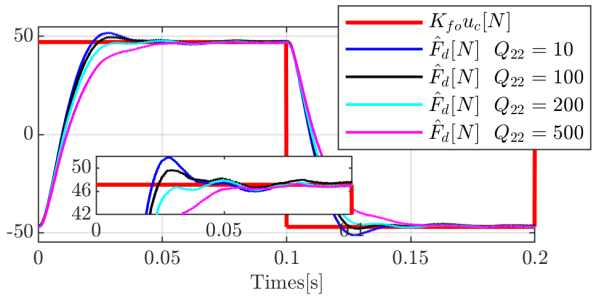

FIGURE 13. The response performance of estimated $\hat{F}_d$ with respect to the injected square-wave disturbance $K_{fo}u_c$ with $Q_{11}=0.01$, $Q_{33}=5e^6$, $R'=1e^{-6}$ and Q_{22} varying within [10, 500].

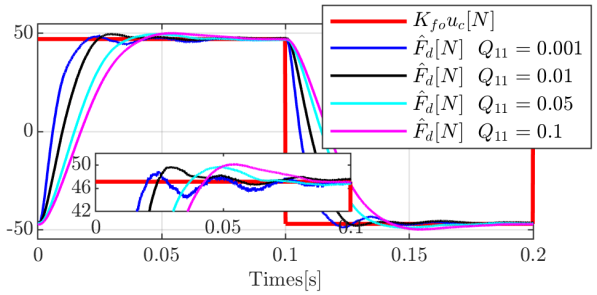

FIGURE 14. The response performance of estimated $\hat{F}_d$ with respect to the injected square-wave disturbance $K_{fo}u_c$ with $Q_{22}=100$, $Q_{33}=5e^6$, $R'=1e^{-6}$ and Q_{11} varying within [0.001, 0.1].

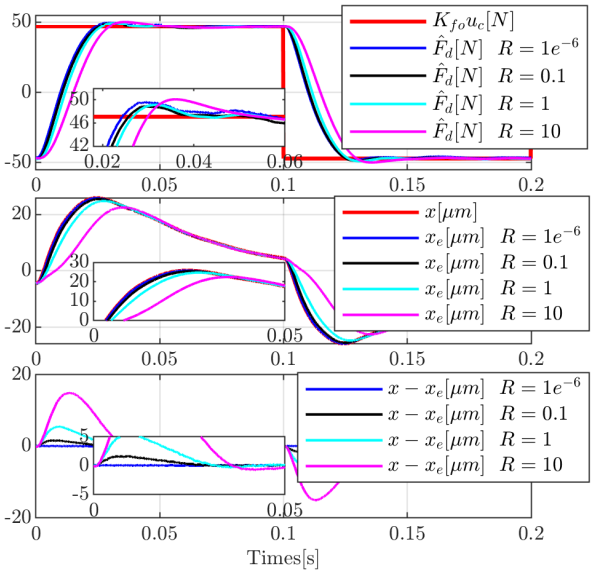

FIGURE 15. The response performance of estimated $\hat{F}_d$, x_e and the position estimation error $x-x_e$ with respect to the injected square-wave disturbance $K_{fo}u_c$ with $Q_{11}=0.01$, $Q_{22}=100$, $Q_{33}=5e^6$ and R' varying within $[1e^{-6}, 10]$.

which is opposite with the effect of Q_{33}. The reason is that Q_{11}, Q_{22} represent the process uncertainty of the previous two equations of (7), i.e., the kinematic equations, so the uncertainty should be low. Thus, increasing the value of Q_{11}, Q_{22} will lower the convergence speed of the estimation of states x, v and then deteriorate the response of $\hat{F}_d$. Fig. 15 shows the response performance of the estimated $\hat{F}_d$, x_e and the position estimation error $x-x_e$ with just changing the parameter R'. It can be clearly indicated that as R' decreases largely, the convergence of $\hat{F}_d, x_e, x-x_e$ also accelerates largely and it can be expected that the response speed will be limited as R' reduces further (for example as it's smaller than $1e^{-6}$). The utilization of high-resolution ($0.1\mu m$) encoder contributes to the little value of R'. The calculation method as shown in [38], i.e., $R'=q^2/12$ is selected where q is the encoder quantization error, can also be directly used here. The calculated result is much below the test range $[1e^{-6}, 10]$, which also validates the effectiveness of the above tuning procedure. Finally, $\boldsymbol{Q}' = \text{diag}\left(0.01, 100, 5e^6\right)$ and $R'=1e^{-6}$ are selected for balancing the speed and overshoot of the state estimation.

Remark 1: The position deviation from the standstill is no more than $\pm 30\mu m$ as depicted in the middle subplot of Fig. 15, so the approximation of (25) is valid. This is also the prerequisite of the proposed tuning method, which can be easily satisfied as the position controller's bandwidth and the magnitude/frequency of the injected square-wave current are both properly selected.

Remark 2: With the above proposed single-variable-method based on the injected square-wave input disturbance, the blind trial-and-error tuning procedure for the KF parameters has been largely released. However, some optimization methods based on explicit performance indices can also be utilized here for more efficient parameter tuning.

Remark 3: The effect of the injected square-wave is equivalent to a sudden load variation as annalyzed in (25). Thus, the effectiveness of the IESM-KF against the load variation can also be verified indirectly with the above tuing results.

4) FORCE RIPPLE COMPENSATION WITH THE IESM-KF

The force ripple compensation results with the proposed IESM-KF are depicted in Fig. 16. It can be seen that, compared with the results in Fig. 11, the maximum tracking error has been largely reduced to about $\pm 0.3\mu m$ (i.e., about 90% reduction) and the magnitudes of the FFT results for the tracking error have been largely deteriorated in the considered frequency range. The detailed comparisons of the estimated force ripple and the tracking error spectrum are listed in Tables. 2 and 3. The force ripple estimation based on the IESM-KF is well consistent with the one estimated from the position controller's output in frequency, but is a little bit different in magnitude as listed in Table. 2. The results with IESM-KF is more accurate due to the further reduction of the position tracking error. The inherent limitations of the feedback control has been released with the IESM-KF-based observer judging from the largely-reduced tracking error.

The variation of the Kalman gains with time is shown in Fig. 17. The convergence time and steady-state value are listed in Table. 4. The gain K_1 converges in one sampling period, which is contributed by the smaller value of R' in (18).

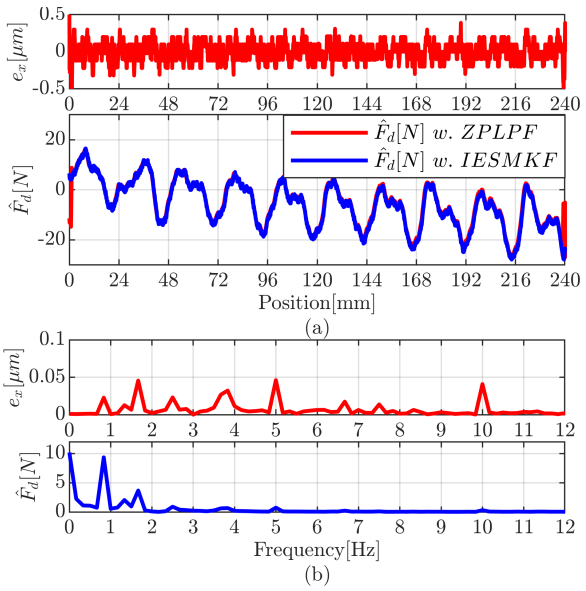

FIGURE 16. Force ripple compensation with IESM-KF. (a) The position tracking error and the estimated force ripple, (b) FFT results of the position error and the estimated force ripple.

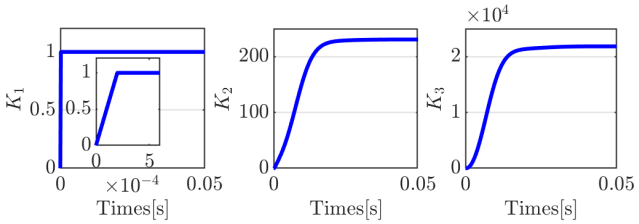

FIGURE 17. The Kalman gain variation of the IESM-KF under $Q' = \text{diag}\left(0.01, 100, 5e^6\right), R' = 1e^{-6}$.

TABLE 3. Comparison of the FFT results for the tracking error with and without the IESM-KF.

Frequency/Hz	Order	Magnitude w.o. IESM-KF(μm)	Magnitude w. IESM-KF(μm)
0.833	1	0.867	0.023
1.333	1.5	0.262	0.013
1.664	2	0.867	0.046
2.494	3	0.232	0.023
3.333	4	0.042	0.006
3.822	4.5	0.233	0.032
4.997	6	0.259	0.046
6.669	8	0.081	0.018
7.516	9	0.039	0.014
9.992	10	0.124	0.041

TABLE 4. Convergence time and steady-state value of the Kalman-Gains.

Kalman Gains	Convergence Time [s]	Steady-state Value
K_1	0.0002	0.9999046
K_2	0.024	230.69394
K_3	0.024	21841.467

The high-precision position measurement makes the value of K_1 approach to unity, which means that the measured position is almost accurate. The convergence time of the gains K_2, K_3 determines the bandwidth of the IESM-KF which can be reduced with increasing the values of Q_{22}, Q_{33} and both balancing the noise effect. With the above tested results, the effectiveness of our proposed IESM-KF-based force ripple estimation/compensation method and the corresponding parameter tuning method have all been verified.

V. CONCLUSION

In this paper, a new force ripple estimation and compensation method has been proposed for the air-bearing PMLSM. The main idea of our proposed method is to model the force ripple as a high-order integrator subsystem when the Coulomb friction in the air-bearing stage is negligible. Based on the idea of the extended state, the lumpded force ripple including the force ripple and the effect of mechanical parameter variation was further modeled as an extra state of the motion system. Then a higher-order extended state model was deduced and the classical Kalman filter theory was utilized to estimate the system states. For further reducing the calculation cost of the Kalman filter as higher-order dynamics of the disturbance was considered, an incremental modeling method was proposed and the computation burden was expected to be largely reduced. Noticing that the parameter tuning of the Kalman filter would be difficult especially as the order increases, a simple and practical parameter tuning scheme was proposed with injecting a square-wave current disturbance to the position controller's output. Moreover, a single-variable-method was used to tune the main parameters with balancing the convergence speed and overshoot of the state estimation and so the blind trial-and-error procedure was avoided. Furthermore, the inevitable time delay of the mechanical system was identified with the sine-sweep model identification method and was furtherly considered in the IESM-KF design. From the experimental results, the effectiveness of our proposed IESM-KF design and the corresponding parameter tuning method has been validated. The proposed incremental extended state modeling method and the parameter tuning scheme can also be expanded to the design and tuning of other obsevers and (or) estimators.

REFERENCES

[1] F. Song, Y. Liu, J. -X. Xu, X. Yang, P. He, and Z. L. Yang, "Iterative learning identification and compensation of space-periodic disturbance in PMLSM systems with time delay," *IEEE Trans. Ind. Electron.*, vol. 65, no. 9, pp. 7579–7589, May 2018.

[2] K. Cho, J. Kim, S. B. Choi, and S. Oh, "A high-precision motion control based on a periodic adaptive disturbance observer in a PMLSM," *IEEE/ASME Trans. Mechatronics*, vol. 20, no. 5, pp. 2158–2171, Oct. 2015.

[3] M. Wang, L. Li, and D. Pan, "Detent force compensation for PMLSM systems based on structural design and control method combination," *IEEE Trans. Ind. Electron.*, vol. 62, no. 11, pp. 6845–6854, Nov. 2015.

[4] Y.-W. Zhu, D.-H. Koo, and Y.-H. Cho, "Detent force minimization of permanent magnet linear synchronous motor by means of two different methods," *IEEE Trans. Magn.*, vol. 44, no. 11, pp. 4345–4348, Nov. 2008.

[5] X. Z. Huang, J. Li, C. Zhang, Z. Y. Qian, L. Y. Li, and D. Gerada, "Electromagnetic and thrust characteristics of double-sided permanent magnet linear synchronous motor adopting staggering primaries structure," *IEEE Trans. Ind. Electron.*, vol. 66, no. 6, pp. 4826–4836, Jun. 2019.

[6] X. Huang, J. Liang, B. Zhou, L. Li, and D. Gerada, "Suppressing the thrust ripple of the consequent-pole permanent magnet linear synchronous motor by two-step design," *IEEE Access*, vol. 6, pp. 32935–32944, Jun. 2018.

[7] Y. W. Zhu and Y. H. Cho, "Thrust ripples suppression of permanent magnet linear synchronous motor," *IEEE Trans. Magn.*, vol. 43, no. 6, pp. 2537–2539, Jun. 2007.

[8] G. Ferretti, G. A. Magnani, and P. Rocco, "Modeling, identification, and compensation of pulsating torque in permanent magnet AC motors," *IEEE Trans. Ind. Electron.*, vol. 45, no. 6, pp. 912–920, Dec. 1998.

[9] C. Rohrig and A. Jochheim, "Identification and compensation of force ripple in linear permanent magnet motors," in *Proc. Amer. Control Conf.*, vol. 3, Jun. 2001, pp. 2161–2166.

[10] C. Rohrig, "Current waveform optimization for force ripple compensation of linear synchronous motors," in *Proc. IEEE Int. Conf. Decis. Control*, Dec. 2003, pp. 5891–5896.

[11] L. Bascetta, P. Rocco, and G. Magnani, "Force ripple compensation in linear motors based on closed-loop position-dependent identification," *IEEE/ASME Trans. Mechatronics*, vol. 15, no. 3, pp. 349–359, Jun. 2010.

[12] B. Grčar, P. Cafuta, G. Štumberger, and A. Stanković, "Control-based reduction of pulsating torque for PMAC machines," *IEEE Trans. Energy Convers.*, vol. 17, no. 2, pp. 169–175, Jun. 2002.

[13] B. E. Helfrich, C. Lee, D. A. Bristow, X. H. Xiao, J. Dong, A. G. Alleyne, S. M. Salapaka, and P. M. Ferreira, "Combined H_∞-feedback control and iterative learning control design with application to nanopositioning systems," *IEEE Trans. Contr. Sys. Technol.*, vol. 18, no. 2, pp. 336–351, Mar. 2010.

[14] M. Lin, Y. Zhu, K. Yang, L. Yang, and C. Hu, "Data-based switching feedforward control for repeating and varying tasks: With application to an ultraprecision wafer stage," *IEEE Trans. Ind. Electron.*, vol. 66, no. 1, pp. 8670–8680, Nov. 2019. doi: 10.1109/TIE.2018.2886804.

[15] Y. Onuki and H. Ishioka, "Compensation for repeatable tracking errors in hard drives using discrete-time repetitive controllers," *IEEE/ASME Trans. Mechatronics*, vol. 6, no. 2, pp. 132–136, Jun. 2001.

[16] H.-S. Ahn, Y. Chen, and H. Dou, "State-periodic adaptive compensation of cogging and Coulomb friction in permanent-magnet linear motors," *IEEE Trans. Magn.*, vol. 41, no. 1, pp. 90–98, Jan. 2005.

[17] Y. Luo, Y. Chen, and Y. G. Pi, "Cogging effect minimization in PMSM position servo system using dual high-order periodic adaptive learning compensation," *ISA Trans.*, vol. 49, no. 4, pp. 479–488, 2010.

[18] K. Ohnishi, M. Shibata, and T. Murakami, "Motion control for advanced mechatronics," *IEEE/ASME Trans. Mechatronics*, vol. 1, no. 1, pp. 56–67, Mar. 1996.

[19] K. K. Tan, S. N. Huang, and T. H. Lee, "Robust adaptive numerical compensation for friction and force ripple in permanent-magnet linear motors," *IEEE Trans. Magn.*, vol. 38, no. 1, pp. 221–228, Jan. 2002.

[20] L. Lu, Z. Chen, B. Yao, and Q. Wang, "Desired compensation adaptive robust control of a linear-motor-driven precision industrial gantry with improved cogging force compensation," *IEEE/ASME Trans. Mechatronics*, vol. 13, no. 6, pp. 617–624, Dec. 2008.

[21] B. Yao, C. X. Hu, L. Lu, and Q. F. Wang, "Adaptive robust precision motion control of a high-speed industrial gantry with cogging force compensations," *IEEE Trans. Control Syst. Technol.*, vol. 19, no. 5, pp. 1149–1159, Sep. 2011.

[22] B. Sencer and E. Shamoto, "Effective torque ripple compensation in feed drive systems based on the adaptive sliding-mode controller," *IEEE/ASME Trans. Mechatronics*, vol. 19, no. 6, pp. 1764–1772, Dec. 2014.

[23] W.-H. Chen, J. Yang, L. Guo, and S. H. Li, "Disturbance-observer-based control and related methods—An overview," *IEEE Trans. Ind. Electron.*, vol. 63, no. 2, pp. 1083–1095, Feb. 2016.

[24] J. Yang, W.-H. Chen, S. H. Li, L. Guo, and Y. Yan, "Disturbance/uncertainty estimation and attenuation techniques in PMSM drives—A survey," *IEEE Trans. Ind. Electron.*, vol. 64, no. 4, pp. 3273–3285, Apr. 2017.

[25] E. Sariyildiz, R. Oboe, and K. Ohnishi, "Disturbance observer-based robust control and its applications: 35^{th} anniversary overview," *IEEE Trans. Ind. Electron.*, to be published. doi: 10.1109/TIE.2019.2903752.

[26] H. Kobayashi, S. Katsura, and K. Ohnishi, "An analysis of parameter variations of disturbance observer for motion control," *IEEE Trans. Ind. Electron.*, vol. 54, no. 6, pp. 3413–3421, Dec. 2007.

[27] H.-W. Chow and N. C. Cheung, "Disturbance and response time improvement of submicrometer precision linear motion system by using modified disturbance compensator and internal model reference control," *IEEE Trans. Ind. Electron.*, vol. 60, no. 1, pp. 139–150, Jan. 2013.

[28] C. J. Kempf and S. Kobayashi, "Disturbance observer and feedforward design for a high-speed direct-drive positioning table," *IEEE Trans. Control Syst. Technol.*, vol. 7, no. 5, pp. 513–526, Sep. 1999.

[29] E. Sariyildiz and K. Ohnishi, "Stability and robustness of disturbance-observer-based motion control systems," *IEEE Trans. Ind. Electron.*, vol. 62, no. 1, pp. 414–422, Jan. 2015.

[30] T. S. Hwang and J. K. Seok, "Observer-based ripple force compensation for linear hybrid stepping motor drives," *IEEE Trans. Ind. Electron.*, vol. 54, no. 5, pp. 2417–2424, Oct. 2007.

[31] F. Auger, M. Hilairet, J. M. Guerrero, E. Monmasson, T. Orlowska-Kowalska, and S. Katsura, "Industrial applications of the Kalman filter: A review," *IEEE Trans. Ind. Electron.*, vol. 60, no. 12, pp. 5458–5471, 2013.

[32] C. Mitsantisuk, K. Ohishi, S. Urushihara, and S. Katsura, "Kalman filter-based disturbance observer and its applications to sensorless force control," *Adv. Robot.*, vol. 25, nos. 3–4, pp. 335–353, Apr. 2011.

[33] C. Mitsantisuk, K. Ohishi, and S. Katsura, "Estimation of action/reaction forces for the bilateral control using Kalman filter," *IEEE Trans. Ind. Electron.*, vol. 59, no. 11, pp. 4383–4393, Nov. 2012.

[34] J. Kim, K. Cho, and S. Choi, "Lumped disturbance compensation using extended Kalman filter for permanent magnet linear motor system," *Int. J. Control, Automa. Sys.*, vol. 14, no. 5, pp. 1244–1253, 2016.

[35] X. Xiao and C. M. Chen, "Reduction of torque ripple due to demagnetization in PMSM using current compensation," *IEEE Trans. Appl. Supercond.*, vol. 20, no. 3, pp. 1068–1071, Jun. 2010.

[36] S. Bolognani, L. Tubiana, and M. Zigliotto, "Extended Kalman filter tuning in sensorless PMSM drives," *IEEE Trans. Ind. Appl.*, vol. 39, no. 6, pp. 1741–1747, Nov./Dec. 2003.

[37] D. Simon, *Optimal State Estimation: Kalman, H Infinity, and Nonlinear Approaches*. Hoboken, NJ, USA: Wiley, 2006.

[38] R. Antonello, K. Ito, and R. Oboe, "Acceleration measurement drift rejection in motion control systems by augmented-state kinematic Kalman filter," *IEEE Trans. Ind. Electron.*, vol. 63, no. 3, pp. 1953–1961, Mar. 2016.

[39] H. Sira-Ramírez, F. González-Montañez, J. A. Cortés-Romero, and A. Luviano-Juárez, "A robust linear field-oriented voltage control for the induction motor: Experimental results," *IEEE Trans. Ind. Electron.*, vol. 60, no. 8, pp. 3025–3033, Aug. 2013.

[40] V. Smidl and Z. Peroutka, "Advantages of square-root extended Kalman filter for sensorless control of AC drives," *IEEE Trans. Ind. Electron.*, vol. 59, no. 11, pp. 4189–4196, Nov. 2012.

[41] H. Butler, "Position control in lithographic equipment [applications of control]," *IEEE Control. Syst. Mag.*, vol. 31, no. 5, pp. 28–47, Oct. 2011.

[42] M. Boutayeb, H. Rafaralahy, and M. Darouach, "Convergence analysis of the extended Kalman filter as an observer for nonlinear discrete-time systems," in *Proc. 34th IEEE Int. Conf. Decis. Control*, Dec. 1995, pp. 1555–1560.

RUI YANG was born in Hubei, China. He received the B.E. degree in electrical engineering from the Harbin Institute of Technology (HIT), Harbin, China, in 2015, where he is currently pursuing the Ph.D. degree.

His research interests include linear motor drive and control, predictive current control, adaptive control, and sliding mode control.

LI-YI LI received the B.E., M.E., and D.E. degrees from the Harbin Institute of Technology (HIT), Harbin, China, in 1991, 1995, and 2001, respectively, where he has been a Professor with the School of Electrical Engineering and Automation, since 2004. In 2013, he became the Yangtze Fund Scholar Distinguished Professor and is currently supported by the National Science Fund for Distinguished Young Scholars. He has authored or coauthored more than 110 technical papers and holds 50 patents.

His research interests include design, drive and control of linear motors, and the design and drive of high-speed/power density permanent magnet machines.

MING-YI WANG was born in Jilin, China. He received the B.E., M.E., and Ph.D. degrees in electrical engineering from the Harbin Institute of Technology (HIT), Harbin, China, in 2009, 2011, and 2016, respectively, where he is currently with the Institute of Electromagnetic and Electronic Technology.

His research interests include motor drive control, power electronic applications, and magnetic levitation.

CHENG-MING ZHANG received the B.E., M.E., and D.E. degrees from the Harbin Institute of Technology (HIT), China, in 2005, 2007, and 2013, respectively, where he has been a Lecturer with the School of Electrical Engineering and Automation, since 2013.

His research interests include the design and drive of linear motors, high efficiency motor systems, and energy conversion and control.

YI-MING ZENG-GU was born in Sichuan, China. He received the B.E. degree in electrical engineering from the Hefei University of Technology (HFUT), Hefei, China, in 2017. He is currently pursuing the M.E. degree in electrical engineering with the Harbin Institute of Technology (HIT).

His research interests include linear motor drive and control, extended Kalman filter, and active disturbance rejection control.